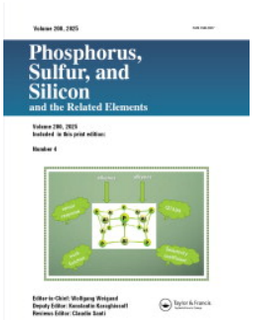

Taylor & Francis
Taylor & Francis Group

Phosphorus, Sulfur, and Silicon and the Related Elements

ISSN: (Print) (Online) Journal homepage: www.tandfonline.com/journals/gpss20

Understanding the reactivity of phosphorus pentasulfide with a series of phosphoryl chloride derivatives: Interplay between σ-hole, π-hole and H-bonding interactions

Pierre Osomba Lohohola, Bienfait Kabuyaya Isamura, Thierry Mawete Dani, Blaise Mbala Mavinga & Jules Tshishimbi Muya

To cite this article: Pierre Osomba Lohohola, Bienfait Kabuyaya Isamura, Thierry Mawete Dani, Blaise Mbala Mavinga & Jules Tshishimbi Muya (04 May 2025): Understanding the reactivity of phosphorus pentasulfide with a series of phosphoryl chloride derivatives: Interplay between σ-hole, π-hole and H-bonding interactions, Phosphorus, Sulfur, and Silicon and the Related Elements, DOI: 10.1080/10426507.2025.2496517

To link to this article: https://doi.org/10.1080/10426507.2025.2496517

PHOSPHORUS, SULFUR, AND SILICON AND THE RELATED ELEMENTS
https://doi.org/10.1080/10426507.2025.2496517

Understanding the reactivity of phosphorus pentasulfide with a series of phosphoryl chloride derivatives: Interplay between σ-hole, π-hole and H-bonding interactions

Pierre Osomba Lohohola[a], Bienfait Kabuyaya Isamura[b,c], Thierry Mawete Dani[a], Blaise Mbala Mavinga[a], and Jules Tshishimbi Muya[a,c]

[a]Department of Chemistry, University of Kinshasa, Kinshasa, Democratic Republic of the Congo; [b]Department of Chemistry, University of Manchester, Manchester, United Kingdom; [c]Research Center for Theoretical Chemistry and Physics, University of Kinshasa, Kinshasa, Democratic Republic of the Congo

ABSTRACT

The reactivity of phosphorus pentasulfide (P_2S_5) in the presence of a series of phosphoryl chloride derivatives has been investigated using the M06-2X and B3LYP functionals in conjunction with the 6-311 + G(d,p) basis set. Our computations indicate that both the regioselectivity of P_2S_5 and the physical nature of the interaction in P_2S_5 complexes can be rationalized using conceptual DFT reactivity indices, natural bond orbitals (NBO) and symmetry-adapted perturbation theory (SAPT2 + dMP2). The molecular electrostatic potential (MEP) of P_2S_5 exhibits σ- and π-hole regions around the P = S bond: one hole is carried by the S atom and located along the P-S bond, while two others are found at both sides of the P atom. Unlike the P_4S_{10} dimer whose reaction is obstructed by a huge activation energy, its monomeric form (P_2S_5) successfully yields a product following a reaction path with a low activation energy and involving metastable complex intermediates. The adducts formed along the P = S unit are less stable than those attacking the P = S bond perpendicularly. The process involves the concomitant weakening of the P···S bond of P_2S_5 and reinforcement of the P=O bond, turning P_2S_5 into P_2S_4O.

ARTICLE HISTORY
Received 2 November 2024
Accepted 13 April 2025

KEYWORDS
Thionation mechanism; phosphorus pentasulfide; conceptual DFT; σ- and π-hole; H-bond

GRAPHICAL ABSTRACT

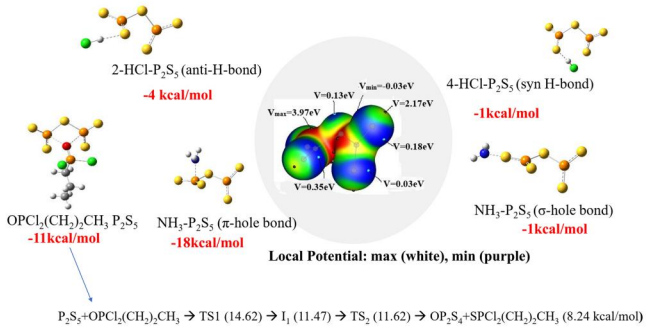

1. Introduction

Phosphorus is an essential element for living organisms, playing an important role in biochemical reactions where it has no substitute.[1] Organophosphorus compounds are used as building blocks and are involved in many biochemical processes and may include both military grade nerve agents and organic pesticides.[2] Those containing the thiophosphoryl group (P = S) are widely used in industrial and environmental applications such as pesticides, extractants for inorganic metal salts, lubricants additives, drugs, and complex-forming agents. Thio-compounds[3,4] are versatile and important intermediates in the synthesis of biologically active molecules. The thionation of a phosphoryl group, i.e. the conversion of a phosphoryl into a thiophosphoryl group, is known as the most efficient way to prepare thiophosphoryl derivatives.[5,6] The synthesis of thionated compounds remains a challenge for synthetic chemists and many reagents have been proposed for thionation including diphosphorus pentasulfide (P_4S_{10}).[7] It is to be noted that when heated at high temperatures, P_4S_{10} decomposes in a variety of P_xS_y compounds with P_2S_5 being the dominant species. Although P_4S_{10} is widely used in organic synthesis, its thionating mechanism is not well documented. Most of

CONTACT Jules Tshishimbi Muya julesmuya.tmuya@gmail.com Department of Chemistry, University of Kinshasa, Kinshasa, Democratic Republic of the Congo.

Supplemental data for this article can be accessed online at https://doi.org/10.1080/10426507.2025.2496517.

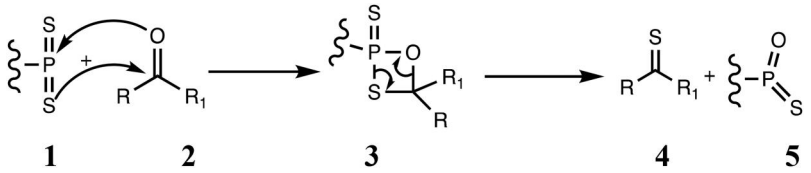

Scheme 1. Thionation mechanism of P_4S_{10}.[7]

the computational mechanistic studies of thionation of carbonyl function reported so far are based on the following mechanism: Scheme 1[7]

This mechanism proposes a decomposition of P_4S_{10} in P_2S_5 (**1**) which attacks the carbonyl functional group (**2**) to form a four-membered ring (**3**) as an intermediate, that afterwards transforms into thioketone (**4**) and more stable compound comprising P=O bond (**5**).

This study focusses on the chemical reactivity of P_2S_5 and thionation mechanism of a phosphoryl group such as $\mathbf{O{=}P}Cl_2CH_2CH_2CH_3$ and attempts to identify key transition states and complexes as intermediates. The three-dimensional structures of P_2S_5-complexes involved as intermediates and P_2S_5 activated states are assumed to be maintained locally by weak non-covalent interactions which contribute to their cohesion.

Non-covalent interactions have gained more significance and are substantially employed in different domains. Among them, the hydrogen bonding[8] is the most investigated and relies on the electrostatic interactions along with induction and dispersion interactions. Studies on sulfur compounds revealed that the anisotropic distribution of the electron density around S is at the basis of their non-covalent bonds' formation.[9] For instance, the electron deficient bivalent sulfur in molecular system has two areas of positive electrostatic potential located along the sigma covalent bonds involving S denoted as σ-hole available for non-covalent interaction with electron donors. Unlike S atom which can bear a positive electrostatic potential in a chemical species along the covalent bond involving S, the electrostatic potential on P atom can lie above and beside the molecular plane. These molecular regions of low electron density are referred as σ- and π-holes when they are either in molecular plane or perpendicular to the planar portion of the molecular frameworks. The σ-holes are also observed in halogen complexes stabilized by the interactions between halogen atoms and the lone pairs of electrons of Lewis bases. This non-covalent bond is referred to halogen-bonding and is located on the part of the surface associated with the halogen atom opposite to covalent halogen bond axis.[10]

In the P_2S_5-$OPCl_2R$ complexes, considered as key intermediate complexes in thionation of $OPCl_2R$ by P_2S_5, the P, S and Cl elements can create competing σ-/π-holes that require a thoroughly investigation. σ-hole, π-hole, and halogen bonds have been subject of study for almost more than two decades. To the best of our knowledge, so far, no studies have been reported on the intermediates formed between P_2S_5 and $OPCl_2R$ based on σ-hole, π -hole, and halogen bonds. The chemical bonding analysis of the $P_2S_5\cdots OPCl_2R$ intermediate complexes is useful in understanding the nature of non-covalent bonding interactions involving Cl, P and S atoms.

The mechanism underlying the formation of non-covalent interactions based on σ- and π -hole concept is well explained by Politzer and Murray.[11] According to these authors, the electron of half-filled atomic p orbital tends to form a covalent bond in between nuclei, thereby reducing the electron density of the outer lobe of the orbital, sitting, either in a covalent bond (σ-hole), or above the covalent bond perpendicular to an atom of a planar molecule (π-hole). Recently, Moradkhani et al.[12] investigated the competition between σ-hole bond, π-hole bond, halogen bond and hydrogen bond in $COCl_2\cdots OCY$ complexes with Y=S, Se, Te and reported the mechanism behind the formation of chalcogen-halogen bonding with OCY as electron-donating species. According to the authors, the strengths of the chalcogen-halogen bond are significantly increased by the σ-holes compare to π-holes. Despite the fact the P_2S_5 is extensively used for thionation of inorganic and organic compounds, the regioselectivity of this thionating agent on phosphoryl group remains uninvestigated. Specifically, this paper explores the competition between σ-hole, π-hole, halogen and hydrogen bonded interactions in the stabilization of $OPCl_2R\cdots P_2S_5$ complexes (R=H, $CH_2CH_2CH_3$) and attempts to elucidate the reaction mechanism of thionation of $OPCl_2CH_2CH_2CH_3$ by P_2S_5.

There is no unique method or procedure to follow in the search for plausible mechanism. This task requires imagination and rigor and the literature abounds with examples of reactions whose mechanisms are considered as well established for many years and have been revised based on quantum chemical methods.[13–16] *Ab initio* calculations are widely used to explore the nature of non-covalent interactions and their influence on the relative stability, molecular physical properties and chemical reaction mechanism of complexes and supramolecular compounds.

2. Results and discussion

2.1. Interactions between P_2S_5 and phosphine oxide derivatives OPR_3 (with R = H, CH_3, F, Cl, Br)

2.1.1. Reactivity descriptors based on conceptual DFT

At elevated temperature, P_4S_{10} quickly transforms in monomeric P_2S_5unit according to:

$$P_4S_{10} \rightarrow 2\ P_2S_5$$

The optimized geometries of P_4S_{10} and P_2S_5 are given in Figure 1. Their computed IR spectra are compared to their experimental ones in Table 1.

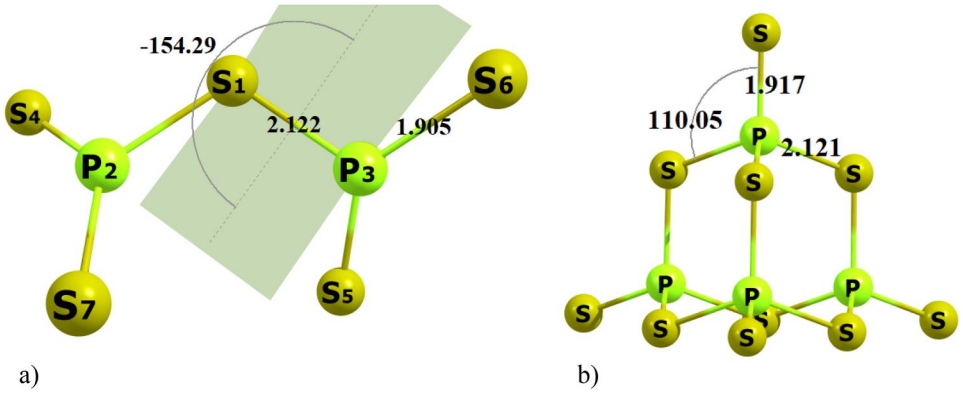

Figure 1. Optimized geometries of P_2S_5 (a) and P_4S_{10} (b).

Table 1. Band assignments of vibrational modes in cm^{-1} for P_4S_{10} and P_2S_5 computed at M06-2X/6-31 + G(d,p) level of theory and corrected by a scaling factor of 0.9522.[25] The experimental data from Ref.[17] are given in parentheses.

P_2S_5	P_4S_{10}	Assignments
782 (690)	686	P=S stretching (t_2 symm)
571 (533)	515	P–S–P stretching symmetric (s) (t_2 symm)
407 (379)	377	P–SP stretching asymmetric (a) (t_2 symm)
220 (264)	258	P–S–P bending (s) (a_1 symm)

(a) and (s) stand for asymmetric and symmetric, respectively.

Table 2. Global reactivity descriptors in eV of P_2S_5 and its dimer P_4S_{10} computed at B3LYP and at M06-2X in parenthesis with 6-311 + G(d,p) level of theory.

	P_2S_5	P_4S_{10}
I	7.64 (6.60)	7.31 (6.25)
A	4.11 (4.69)	2.78 (3.26)
μ	−5.88 (-5.65)	−5.05 (−4.76)
H	3.53 (1.91)	4.53 (2.99)
Ω	4.89 (8.34)	2.81 (3.78)
ω^-	12.94 (19.63)	8.42 (10.13)
ω^+	7.06 (13.98)	3.38 (5.37)
A/I	0.54 (0.71)	0.38 (0.52)
$\Delta\omega$	−5.88 (−5.05)	−5.65 (−4.76)

To understand the global reactivity of P_2S_5 and P_4S_{10}, global reactivity descriptors such as electronegativity (χ), chemical potential (μ), hardness (η), electron donor ability (ω^-) and electron acceptor properties (ω^+) of P_2S_5 and P_4S_{10} were evaluated at B3LYP and M06-2X theory levels. These conceptual DFT based reactivity descriptors were computed by considering the Koopman's theorem approach where the negative HOMO and LUMO energies (ε_H and ε_L) are approximated as ionization energy (I) and electron affinity (A), respectively, as:

$$\chi = -\mu = 1/2\ (\varepsilon_L + \varepsilon_H) \quad (1)$$

$$\eta \approx (\varepsilon_L - \varepsilon_H) \quad (2)$$

$$\omega\ = (\varepsilon_L + \varepsilon_H)^2/2\ (\varepsilon_L - \varepsilon_H) \quad (3)$$

$$\omega^- = (3\ I\ +\ A)^2/16\ (I\ -\ A) \quad (4)$$

$$\omega^+ = (I\ +\ 3\ A)^2/16\ (I\ -\ A) \quad (5)$$

The global reactivity descriptors of P_2S_5 and those of its dimer P_4S_{10} computed at B3LYP and M06-2X levels of theory are provided in Table 2. The absolute values of the electronegativity, chemical hardness, electrophilicity, chemical potential, and electron donating and electron accepting powers computed at B3LYP and M06-2X levels of theory predict P_2S_5 to be more reactive than its dimer P_4S_{10} with an electron affinity and an electron donating power of 4.11 and 12.94 eV, respectively (4.69 and 19.63 eV at M06-2X). P_2S_5 has a propensity of receiving and donating electrons. The electron accepting and electron donating power energy difference of P_2S_5 computed at B3LYP level of theory amounts to −5.88 eV ($\Delta\omega$ = −5.05 eV at M06-2X level of theory). This character is even higher in P_2S_5 than in P_4S_{10}, the former being harder than the latter.

To check the regioselectivity of these compounds local reactivity descriptors, namely frontier molecular orbitals, and molecular electrostatic potentials were computed at M06-2X/6-31 + G(d,p). The results obtained are depicted in Figure 2. The HOMO suggests that S is the preferred site for electrophilic attacks while the LUMO prefers nucleophilic attacks on both sites (S and P). The MEP shows that the electron density is higher in the surrounding of sulfur atoms while electron-poor regions are observed along the P-S axis on S and above the molecular plane on P. In accordance with the literature, these electron deficient sites are denoted in the present paper as σ- and π-holes, respectively, indicating that both sites can interact in a highly directional manner with electron-rich species, such as $OPCl_2CH_2CH_2Cl$. The locations of the minima and extrema on the molecular electrostatic potential of P_2S_5 and their values computed using FWA program[18] are given in Figures 3 and S1 and Tables 3 and S1.

The values of the electrostatic potential of P_2S_5 on the map depicted in Figure 3 show regions where the electron density either diminishes or increases. These regions are predicted to interact favorably with negative or positive sites of $OPCl_2R$ molecule.

The maxima are localized mostly on phosphorus ($V_{s,max}$ = 3.97 eV) while the minima are on sulfur ($V_{s,min}$ = −0.03 eV). The positive π-hole region located on P is much lower in electron density than the σ-hole on S (V_s = 2.12 eV). According to the location of stationary points on the landscape of P_2S_5 MEP, it was anticipated that electrophilic fragments would attack the sulfur atom through the sites 3, 4 or 1, 2. These two different orientations are

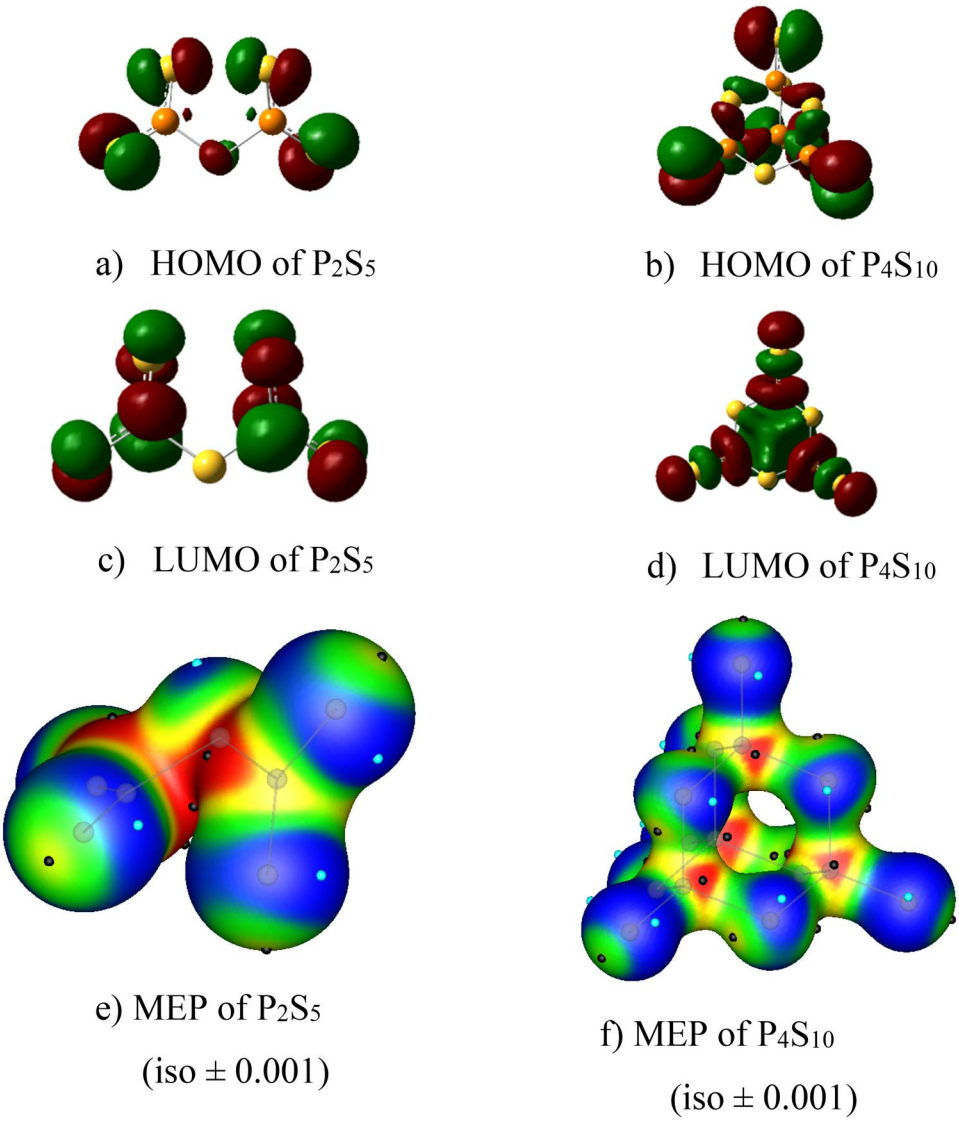

Figure 2. Frontier molecular orbitals, and molecular electrostatic potentials of the P_2S_5 and dimer P_4S_{10} computed at M06-2X/6-31 + G(d,p) level of theory. In this map, red and blue represent the maximum positive and minimum potential, which varies in the following order: red > yellow > green > blue.

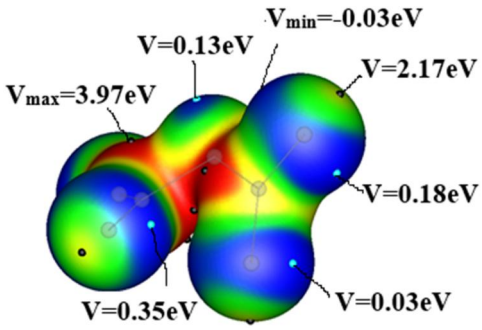

Figure 3. Values of the maxima (red) and minima (blue) of the electrostatic potential of P_2S_5 computed at M06-2X/6-31 + G(d,p) level of theory.

Table 3. The number of minima ($V_{s,min}$ in blue) and maxima ($V_{s,max}$ in red) of the electrostatic potential surface and their values in eV.

# sites	$V_{s,min}$	$V_{s,max}$	# sites
1	0.18	–	
2	0.03	–	
3	−0.03	–	
4	0.35	–	
5	–	2.12	
6	–	3.97	
7	0.62	3.86	

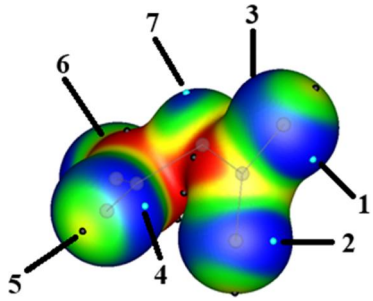

referred to in this work as anti- (Figures 4(a and b)) and syn-attack (Figures 4(c and d)). The most favorable site for electrophilic attack is predicted to be on site 3 assuming that the potential in this local region is the lowest (global minimum) controlled by S and indicates the most negatively charged local site.

On the other hand, nucleophilic entities are likely to bind onto the σ- and π-holes ($V_{s,max}$ = 2.12; 3.97 eV), which correspond to the maxima electrostatic potentials on S and P atoms. To probe the chemical regioselectivity of different reactive sites predicted by conceptual DFT descriptors, the

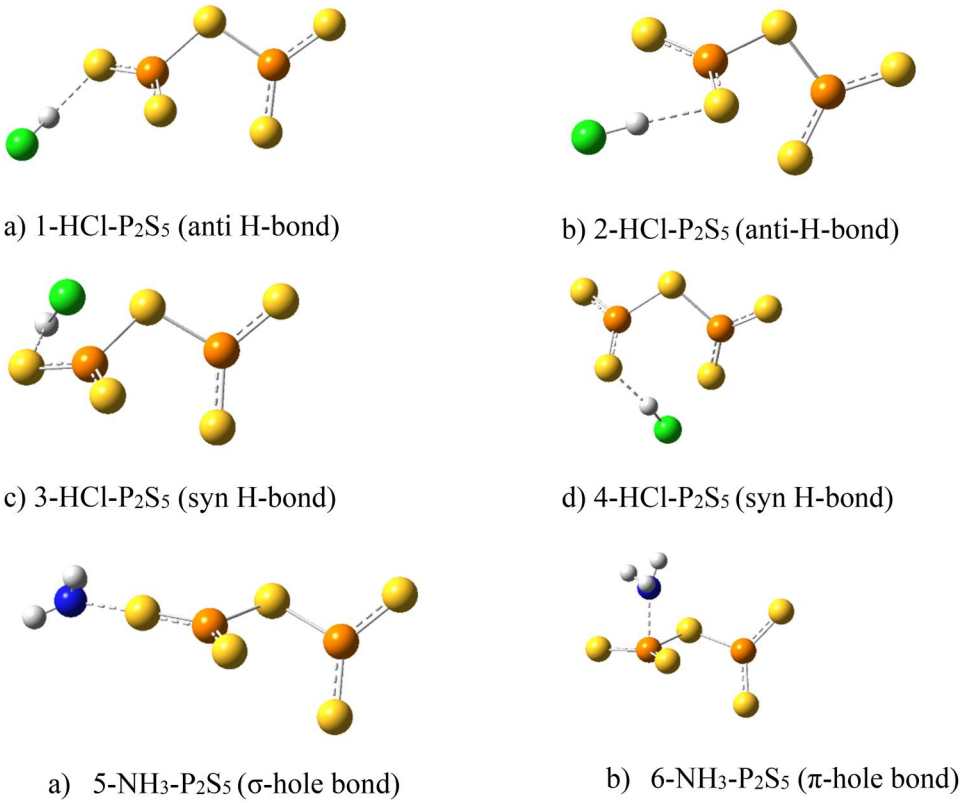

Figure 4. Different modes of interactions (sites identified by labels 1–6) were employed in the present paper illustrating H-bond, σ- and π-hole bonds based on conceptual DFT predictions.

binding energies of the complexes formed between P_2S_5 with XH_3, POX_2H, and $POCl_2CH_2CH_2CH_3$ (X = N, P) were computed at M06-2X/6-311 + G(d,p) level of theory. The initial geometries showing different modes of interactions considered in the present work, based on conceptual DFT predictions, are shown in Figure 4.

2.1.2. Binding energies between P_2S_5 and phosphine oxide derivatives (OPR_3)

The hydrogen-, halogen- and chalcogen-bonded interaction between P_2S_5 with both electron donor (NH_3, PH_3, $OPCl_2H$ and $OPCl_2CH_2CH_2CH_3$) and acceptor (HCl) are chosen to probe the reactivity of P_2S_5. The optimized geometries of X-P_2S_5 (X = HCl, NH_3, PH_3, $OPCl_2H$, $OPCl_2CH_2CH_2CH_3$) complexes are shown in Figure 5 and Figure S1. Their binding energies computed as electronic energy differences between the complexes and their components including zero-point energies and basis set superposition errors corrections along with the interaction energies are listed in Table 4.

The S-P-S-P torsional angle in 1-HCl- and 2-HCl-complexes is nearly ± 30°, and tends to ± 90° in 3-HCl- and 4-HCl-complexes. The intermolecular S···H-Cl bond in 1-HCl-complex and 2-HCl-complex is estimated to about 2.63 Å, which is 0.05 Å longer than that in 3-HCl-complex and 4-HCl-complex. The 7-HCl-complex is not viable and relaxed toward 3-HCl-complex or 4-HCl-complex. The 6-NH_3-P_2S_5 and 6-PH_3-P_2S_5 optimized geometries are characterized by a N···P and P···P intermolecular bonds of 1.94 and 2.50 Å, which are 1.16 and 1.28 Å shorter than that of 5-NH_3-P_2S_5 and 5-PH_3-P_2S_5. All the optimized geometries of these complexes are provided in Figure S1. Figure 5 depicts the equilibrium geometries of P_2S_5-$OPCl_2R$ complexes (with R = H, $CH_2CH_2CH_3$). The optimized geometries of $OPCl_2H$-P_2S_5 complexes show that $OPCl_2H$ tends to form short SP···O intermolecular bonds of ∼ 1.95 Å, while the S = P···Cl and P = S···H bond distances are ranged around 3.51 and 2.86 Å. The $OPCl_2H$-P_2S_5 complex tends to combine both π -hole on P and hydrogen bond. It is to be noted that the S = P···Cl bond distance in $OPCl_2H$-P_2S_5 complex is ∼0.1 Å shorter than the sum of the van der Waals radii of P and Cl atoms (3.6 Å)[19], indicating the formation of a weak complex.

The binding energies corrected by zero-point energies and basis set superposition error energies of these complexes are listed in Table 4. According to the binding energies of HCl, the *syn* orientation is more preferential for electrophilic attacks than the *anti*-orientation as referred to their relative stability of nearly 2.4 kcal/mol compared to *anti*-HCl-P_2S_5 complexes. In contrast, the σ-hole interaction with NH_3 is weaker than the π-hole interaction and amounts, respectively, to −1.42 and −18.04 kcal/mol. The P site is confirmed to be a hard site as it establishes a stronger interaction with NH_3 as compared to PH_3. The BSSE corrections in HCl-P_2S_5 complexes are smaller as compare to those of NH_3-P_2S_5 and PH_3-P_2S_5 complexes. The regioselectivity of P_2S_5 was also probed using O = PCl_2H and 4-$OPCl_2CH_2CH_2CH_3$.

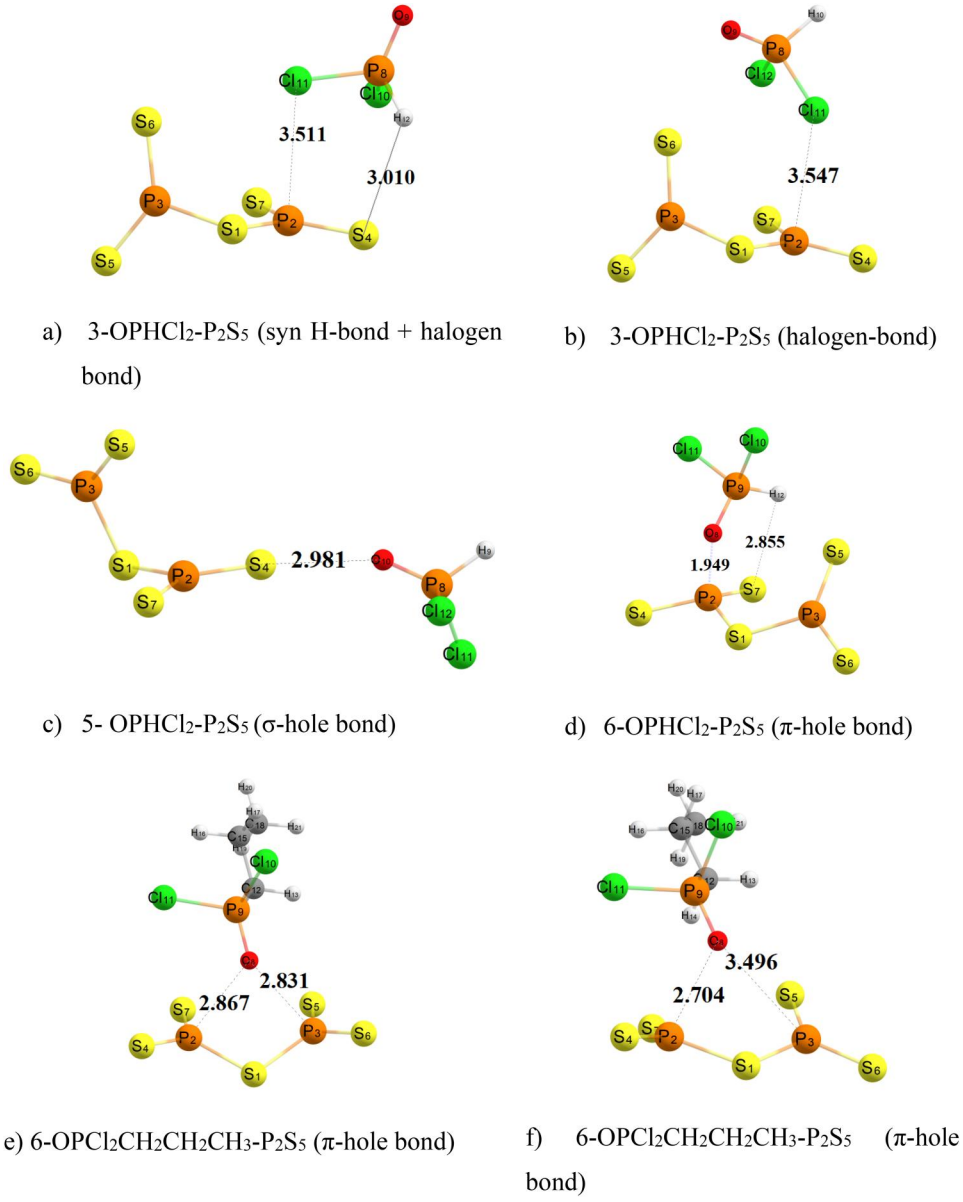

a) 3-$OPHCl_2$-P_2S_5 (syn H-bond + halogen bond)

b) 3-$OPHCl_2$-P_2S_5 (halogen-bond)

c) 5- $OPHCl_2$-P_2S_5 (σ-hole bond)

d) 6-$OPHCl_2$-P_2S_5 (π-hole bond)

e) 6-$OPCl_2CH_2CH_2CH_3$-P_2S_5 (π-hole bond)

f) 6-$OPCl_2CH_2CH_2CH_3$-P_2S_5 (π-hole bond)

Figure 5. Optimized geometries of $OPHCl_2$-P_2S_5 and $OPCl_2CH_2CH_2CH_3$-P_2S_5 complexes computed at M06-2X/6-311 + G(d,p) levels of theory.

Table 4. Binding energies of complexes (BE) between P_2S_5 with HCl, NH_3 and PH_3 computed at M06-2X and at 6-311 + G(d,p) level of theory and the interaction energies (IE) including the basis-superposition errors (BSSE) and zero-point energies (ZPE) corrections in kcal/mol.

Complexes	BE	BE+BSSE	BE+BSSE+ZPE	BE+ZPE	BSSE	IE
1-HCl-P_2S_5	−2.84	−2.18	−1.24	−1.89	0.65	−2.25
2-HCl-P_2S_5	−2.85	−2.18	−1.24	−1.89	0.65	−2.25
3-HCl-P_2S_5	−5.49	−4.39	−3.59	−4.69	1.11	−4.60
4-HCl-P_2S_5	−5.06	−4.39	−3.59	−4.26	0.68	−4.60
5-NH_3-P_2S_5	−2.78	−2.03	−1.42	−2.16	0.74	−2.12
6-NH_3-P_2S_5	−26.34	−21.87	−18.04	−22.52	4.47	−30.48
5-PH_3-P_2S_5	9.93	10.44	10.27	9.77	0.51	−0.64
6-PH_3-P_2S_5	−8.32	−5.53	−3.79	−6.58	2.79	−16.24

The modes of interactions are identified by labels 1-6.

Table 5. Binding energies (in kcal/mol) of $OPHCl_2$-P_2S_5 and $OPCl_2CH_2CH_2CH_3$-P_2S_5 complexes.

Complexes	Bond type	BE+BSSE	BE+ZPE +BSSE	BSSE
3- $OPHCl_2$-P_2S_5	H-bond (*syn*)	−2.69	−2.51	2.17
3-$OPHCl_2$-P_2S_5	halogen-bond (*syn*)	−5.24	−4.80	3.11
5- $OPHCl_2$-P_2S_5	σ-hole bond	−4.34	−3.90	2.62
6-$OPHCl_2$-P_2S_5	π-hole bond	−9.45	−8.87	3.79
6-$OPCl_2CH_2CH_2CH_3$-P_2S_5	π-hole bond(a)	−11.34	−10.63	5.66
6-$OPCl_2CH_2CH_2CH_3$-P_2S_5	π-hole bond (b)	−10.13	−8.94	4.96

In which a and b refer to structures of complexes depicted in Figure 5(e and f), respectively.

Note that both compounds can bind to P_2S_5 through various modes, depending on the orientation and electronic character of the atoms involved in the interaction.

Electronegative atoms such as sulfur can act as positive σ-hole pair interactions. The optimized geometries and the binding energies including BSSE and ZPE corrections of $O=PCl_2H$ and $O=PCl_2CH_2CH_2CH_3$ complexes are given in Figure 5 and Table 5. The π-hole located on the phosphor site of P_2S_5 is more reactive as illustrated by its binding energy with $OPHCl_2$ of −8.87 kcal/mol compared to σ-hole interaction on S (BE = −3.90 kcal/mol), halogen bonding interaction (BE = −4.80 kcal/mol) and hydrogen bond (BE = −2.51 kcal/mol). As $OPHCl_2$ plays the role of

Table 6. Natural bond orbital analysis of various systems of interest. The overall charge transfer (CT) between the two fragments is expressed in electrons, while second-order perturbation energies are given in kcal/mol. Only interactions with $E^{(2)}$ greater than 1 kcal/mol are reported.

System	Orbital interaction	Direction	$E^{(2)}$	CT
	LP(O8) → σ*(P2-S4)	$OPHCl_2 \rightarrow P_2S_5$	105.6	
$OPHCl_2$	LP(O8) → σ*(P1-S2)	$OPHCl_2 \rightarrow P_2S_5$	16.26	0.154
	LP(O8) → σ*(P2-S7)	$OPHCl_2 \rightarrow P_2S_5$	4.66	
	LP(O8) → σ*(P2- S1)	$OPCl_2R \rightarrow P_2S_5$	17.96	
$OPCl_2R$-P_2S_5	LP(O8) → σ*(P2-S4)	$OPCl_2R \rightarrow P_2S_5$	103.41	0.162
	LP(O8) → σ*(P2-S7)	$OPCl_2R \rightarrow P_2S_5$	2.93	

$R = CH_2CH_2CH_3$.

Table 7. SAPT2 + dMP2 energy analysis of the interaction energy of the complex between $OPHCl_2$ and P_2S_5. All energy terms are given in kcal/mol and were computed at the SAPT2 + dMP2/aug-cc-pVDZ level of theory as implemented in the Psi4 python package.

Energy terms	Nature	Value
Electrostatic	Attractive	−85.27
Induction	Attractive	−53.33
Dispersion	Attractive	−30.92
Exchange	Repulsive	157.66
Total	Attractive	−11.86

electron-donating entity, substituting H by the $CH_2CH_2CH_3$ group increases its donating power (BE = −10.63 kcal/mol). The relative stabilities of these complexes based on the computed binding energies are in good agreement with the calculated intermolecular bond lengths of the optimized geometries of complexes.

2.2. Chemical bonding and energy decomposition analysis

2.2.1. Chemical bonding analysis via natural bond orbitals

Second-order perturbation theory analyses of the Fock matrix in terms of natural bond orbital (NBO) basis were performed for the most stable $OPHCl_2$-P_2S_5 and $OPCl_2CH_2CH_2CH_3$-P_2S_5 complexes. The results summarized in Table 6 suggest that the π-hole bonded $OPHCl_2$-P_2S_5 complex experiences a charge transfer of 0.154 e^-, an observation that aligns with the strong asymmetry of the bidirectional orbital interactions between the two fragments. Indeed, transitions originating from donor NBOs located on $OPHCl_2$ are up to an order of magnitude more intense than those stemming from NBOs of P_2S_5 donor. Furthermore, the fact that the overall loss of electron density occurs on the $OPHCl_2$ fragment corroborates the higher nucleophilic character of this moiety as compared to P_2S_5. It is worth highlighting that the strongest interaction between donor and acceptor NBOs was associated with an $E^{(2)}$ value of ∼106 kcal/mol and involved the lone pairs of O8 and the antibonding σ* (P-S) NBO.

Similarly, complex $OPCl_2R$-P_2S_5 (Figure 5(f)) also experiences a charge transfer as large as 0.162 e^-, which flows overall from $OPCl_2R$ to P_2S_5. The excess density of 0.008 e^- reflects the higher donating power of $OPCl_2R$ as compared to $OPHCl_2$ caused by the substitution of the H atom by the aliphatic -$CH_2CH_2CH_3$ group. The interaction between the donor NBO lone pairs of O8 and the antibonding σ* (P2-S4) orbital is once again found to be the strongest with an $E^{(2)}$ estimated at 103 kcal/mol. Several orbital interactions involving the R group were also observed. Despite being relatively weak, these transitions must have contributed to the pronounced stability of $OPCl_2R$-P_2S_5 as compared to $OPHCl_2$-P_2S_5.

2.2.2. Symmetry adapted perturbation theory (SAPT2 + dMP2) analysis

The data in Table 7 suggest that the 6-$OPHCl_2$-P_2S_5 complex is mainly stabilized by electrostatic interactions, which are assisted by non-negligible inductive and dispersive effects. The significant contribution of the previous non-electrostatic effects on the overall stability of the complex is consistent with NBO calculations which indicated a significant charge transfer (>0.15 e^-) between occupied and unoccupied natural bond orbitals of the constituting fragments. Despite the large exchange repulsion of ∼158 kcal/mol, which tends to destabilize the system, the overall interaction energy is attractive and estimated at ∼12 kcal/mol.

2.3. Kinetic analysis of the formation of $SPCl_2CH_2CH_2CH_3$

The transformation of $OPCl(CH_2)_2CH_3$ in $SPCl(CH_2)_2CH_3$ through P_4S_{10} takes place in multiple steps. First, the P_4S_{10} dimer is converted by heating into P_2S_5 monomer. Next the $OPCl_2(CH_2)_2CH_3$ attacks the P_2S_5 and forms an intermediate complex (**I1**) laying 11.47 kcal/mol above the reagents *via* a high energy transition state (**TS1**) located at 14.62 kcal/mol. Then, the **I1** complex passes through an unstable structure, a barrier-less transition state (**TS2**), situated at 11.62 kcal/mol that transforms without activation energy in the intermediate complex **I2** that immediately transforms finally into OP_2S_4 and $SPCl_2(CH_2)_2CH_3$:

$$P_2S_5 + OPCl_2(CH_2)_2CH_3 \rightarrow \mathbf{TS1}(14.62) \rightarrow \mathbf{I1}(11.47) \rightarrow \mathbf{TS2}(11.62) \rightarrow \mathbf{I2}(8.24) \rightarrow OP_2S_4 + SPCl_2(CH_2)_2CH_3$$

The relative energies and geometries of the transition states and intermediates involved in the reaction mechanism of the conversion of $OPCl_2(CH_2)_2CH_3$ in $SPCl_2(CH_2)_2CH_3$ are shown in Figure 6. The imaginary vibrational modes of the transition states (**TS1** and **TS2**) and the intrinsic reaction coordinate scan graphs illustrating the connection of **TS1** and **TS2** states with the **I2** and the final product computed at M06-2X/6-311 + G(d,p) levels of theory are shown in Figure S2.

The first step is kinetically determinant. The theoretical data of the reaction mechanism showed that P_4S_{10} cannot react in its dimeric form due to the large energy barrier that must be overcome (around 254 kcal/mol). The product is thermodynamically 8.2 kcal/mol less stable than the reactants but it is predicted kinetically to be formed faster due to the small barrier between the **I2** and **TS2**. This result is in good agreement with our experimental findings.

2.4. Experimental NMR data for propylthiophosphonic dichloride ($SPCl_2(CH_2)_2CH_3$)

After reaction, the $SPCl_2(CH_2)_2CH_3$ product was isolated as colorless liquid in 61% yield with the following features: ^1H

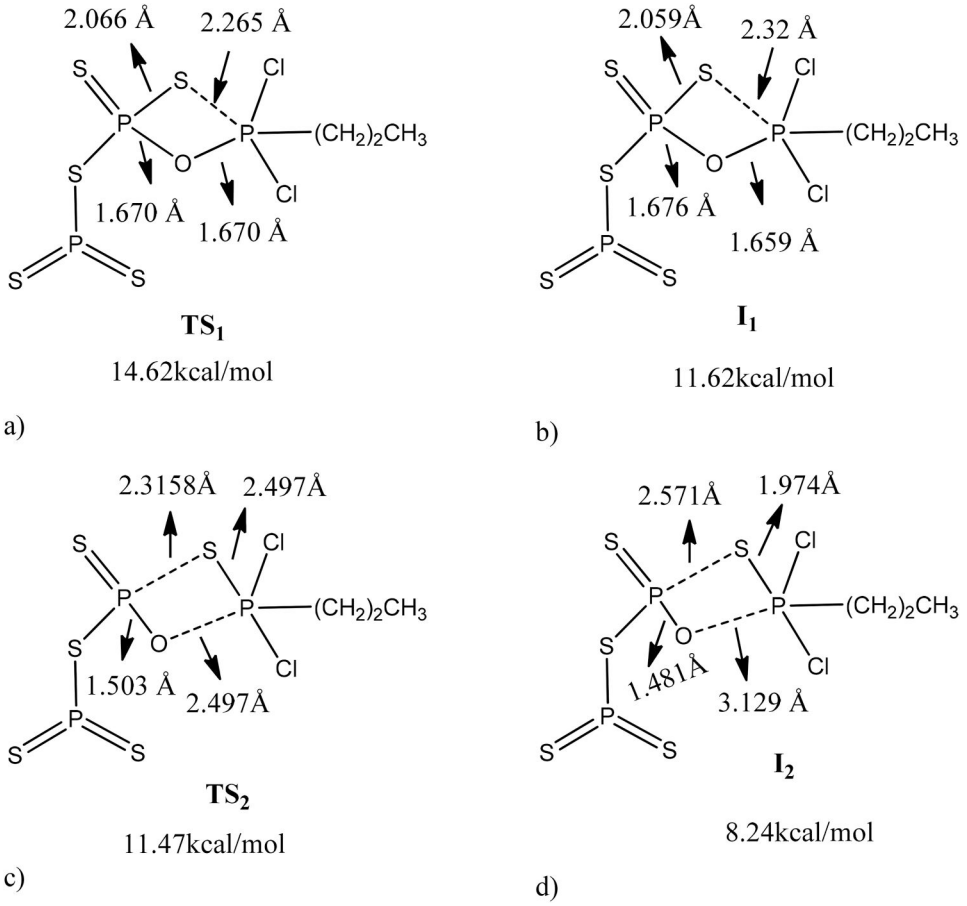

Figure 6. Relative energies and geometrical parameters of chemical species involved in the transformation of $OPCl_2R$ into $SPCl_2R$ with $R = CH_2CH_2CH_3$ computed at M06-2X/6-31 + G(d,p) levels of theory: (a,c) transition states and (b,d) intermediate and products.

NMR (400 MHz, $CDCl_3$): δ = 1.13 (m, 3H), 1.95 (m, 2H), 2.72 (m, 2H).^{13}C NMR (100 MHz, $CDCl_3$): δ = 14.2, 17.9, 52.0.^{31}P NMR (162 MHz, $CDCl_3$): δ = 91.3.

$$\text{MS}: \ m/z = 176 \ [M^+].$$

3. Computational and experimental details

3.1. Computational details

The B3LYP and M06-2X[20] functionals were utilized in conjunction with the 6-31 + G(d,p) basis set[21] to investigate the mechanism of the reaction between $CH_3CH_2CH_2POCl_2$, and P_2S_5 in the gas phase, keeping in mind the fact that P_4S_{10} is unstable at high temperature and decomposes in P_2S_5. The chemical regioselectivity of P_2S_5 was predicted based on conceptual density functional theory (CDFT) descriptors.[22] Note that these chemical species are intriguing due to the presence of local sites (S and P) that can act as both nucleophiles and electrophiles. The molecular electrostatic potential was computed and visualized using the wave function analysis-surface suite (WFA-SAS) program[18] with no constrained symmetry and 6 d and 10 f Cartesian functions. The sites predicted by CDFT descriptors were then chosen to build and compute the binding energies of $P_2S_5\cdots XH_3$, $P_2S_5\cdots POX_2H$ and $POCl_2CH_2CH_2CH_3$ complexes at M06-2X/6-311 + G(d,p) levels of theory including basis set superposition (BSSE)[23] and zero point energies (ZPE)[24] corrections. To elucidate the thionation process of $OPOCl_2CH_2CH_2CH_3$ by P_2S_5 reagent, energy barriers and reaction energies were calculated at M06-2X/6-31 + G(d,p) levels of theory. These analyses were complemented by natural bond orbital (NBO)[25] and symmetry adapted perturbation theory (SAPT2 + dMP2/aug-cc-pVDZ)[26] calculations aimed at rationalizing the chemical bonding of reaction intermediates. All the species were optimized and their geometries were confirmed to be either minima or maxima on their respective potential energy surfaces through vibrational frequency calculations. All vibrational frequencies reported in the present study were corrected by a scaling factor of 0.9522 as suggested by the computational chemistry comparison and benchmark data base.[27] Gaussian 16 program[28] was used for the calculations. For visualization purposes, Gauss View 6.0 and Chemcraft software were employed.[29,30]

3.2. Experimental details

$OPCl_2CH_2CH_2CH_3$ was experimentally converted in $SPOCl_2CH_2CH_2CH_3$ employing P_4S_{10} reagent at high temperature. The NMR spectra of $POCl_2CH_2CH_2CH_3$ and that of $SPOCl_2CH_2CH_2CH_3$ were recorded for their characterization. All reagents and solvents were used without further purification. The spectra were recorded with a Bruker Ascend 400 spectrometer[31] operating at 400 MHz, 100 MHz

and 162 MHz for ^{1}H, ^{13}C and ^{31}P, respectively, in $CDCl_3$ using tetramethylsilane as internal reference. The values of chemical shifts are reported relative to tetramethylsilane and H_3PO_4 in ppm.

Conclusion

The chemical regioselectivity of P_2S_5, its non-covalent hole interactions ability, and its reaction mechanism of thionation with $OPCl_2CH_2CH_2CH_3$ have been investigated using conceptual DFT descriptors, NBO and SAPT2 + dMP2. Our results show that P_2S_5 can react with both acid and base but has a higher propensity to receiving than donating its electrons. The MEP plot of P_2S_5 shows one σ-hole on S and two π-holes at both sides of P indicating that both atoms can interact with nucleophiles. Acids prefer to interact with the S atom of P_2S_5 in syn orientation while hard bases prefer P forming more stable π-holes bonded complexes. The π-hole interaction stabilizes more $OPRCl_2$-P_2S_5 complexes as illustrated by its binding energy with $OPHCl_2$ of −8.87 kcal/mol (−10.63 kcal/mol for $OPCl_2CH_2CH_2CH_3$-P_2S_5 π-hole bonded complex) compared to that of σ-hole bond, halogen bond and hydrogen bond estimated to −3.90, −4.80 and −2.51 kcal/mol, respectively. Finally, the transformation of $OPClCH_2CH_2CH_3$ in $SPClCH_2CH_2CH_3$ through P_4S_{10} takes place as follows: P_2S_5 + $OPCl_2(CH_2)_2CH_3$ → **TS1** (14.62) → **I1** (11.47) → **TS2** (11.62) → OP_2S_4 + $SPCl_2(CH_2)_2CH_3$ (8.24).

Acknowledgments

JTM thanks Professor Carol Parish, the University of Richmond and the Fulbright program for a short research stay and financial support, and the VLIR-UOS program and professor Daniels Escudero from KU Leuven.

Author contributions

The manuscript was written through the contribution of all authors and the latter approved the final version.

P. Osomba Lohohola: contributed to project conceptualization; supervised the project, and validated experimental and theoretical data

B. K. Isamura: Carried out SAPT calculations, edited the paper, and contributed to data analysis

D. Mawete: carried out experimental data and contributed to the discussion

B. Mbala: Reviewed the paper and contributed to project conceptualization

J. T. Muya: performed most of the calculations, edited the paper, analyzed the data, contributed to project conceptualization and funding acquisition.

All the authors have seen and approved the current manuscript.

Disclosure statement

The authors declare no competing interests.

ORCID

Bienfait Kabuyaya Isamura http://orcid.org/0000-0003-3278-3284
Blaise Mbala Mavinga http://orcid.org/0000-0001-8020-6700
Jules Tshishimbi Muya http://orcid.org/0000-0003-4527-2619

Data availability statement

The authors declare that the data supporting the findings of this study are available within the paper and its Supplementary Information files. Should any raw data files be needed in another format they are available from the corresponding author upon reasonable request.

Funding

Fulbright program.

References

[1] Gibard, C.; Bhowmik, S.; Karki, M.; Kim, E.-K.; Krishnamurthy, R. Phosphorylation, Oligomerization and Self-Assembly in Water under Potential Prebiotic Conditions. *Nat. Chem.* **2018**, *10*, 212–217. DOI: 10.1038/nchem.2878.

[2] Mahammed, K.; Jayashankara, V.; Premsai Rai, N.; Mohana Raju, K.; Arunachalam, P. A Mild and Versatile Synthesis of Thioamides. *Synlett* **2009**, *2009*, 2338–2340. DOI: 10.1055/s-0029-1217711.

[3] Cao, X.-T.; Qiao, L.; Zheng, H.; Yang, H.-Y.; Zhang, P.-F. A Efficient Protocol for the Synthesis of Thioamides in [DBUH][OAc] at Room Temperature. *RSC Adv.* **2018**, *8*, 170–175. DOI: 10.1039/C7RA11259A.

[4] Polshettiwar, V.; Kaushik, M. P. Recent Advances in Thionating Reagents for the Synthesis of Organosulfur Compounds. *J. Sulfur Chem.* **2006**, *27*, 353–386. DOI: 10.1080/17415990600733112.

[5] Curphey, T. J. Thionation with the Reagent Combination of Phosphorus Pentasulfide and Hexamethyldisiloxane. *J. Org. Chem.* **2002**, *67*, 6461–6473. DOI: 10.1021/jo0256742.

[6] Brillon, D. Recent Developments in the Area of Thionation Methods and Related Synthetic Applications. *Sulfur Rep.* **1992**, *12*, 297–332. DOI: 10.1080/01961779208048946.

[7] Ozturk, T.; Ertas, E.; Mert, O. A Berzelius Reagent, Phosphorus Decasulfide (P_4S_{10}), in Organic Syntheses. *Chem. Rev.* **2010**, *110*, 3419–3478. DOI: 10.1021/cr900243d.

[8] Scheiner, S. The Hydrogen Bond: A Hundred Years and Counting. *J. Indian Inst. Sci.* **2020**, *100*, 61–76. DOI: 10.1007/s41745-019-00142-8.

[9] Scilabra, P.; Terraneo, G.; Resnati, G. The Chalcogen Bond in Crystalline Solids: A World Parallel to Halogen Bond. *Acc. Chem. Res.* **2019**, *52*, 1313–1324. DOI: 10.1021/acs.accounts.9b00037.

[10] Cavallo, G.; Metrangolo, P.; Milani, R.; Pilati, T.; Priimagi, A.; Resnati, G.; Terraneo, G. The Halogen Bond. *Chem. Rev.* **2016**, *116*, 2478–2601. DOI: 10.1021/acs.chemrev.5b00484.

[11] Politzer, P.; Murray, J. S.; Clark, T.; Resnati, G. The σ-Hole Revisited. *Phys. Chem. Chem. Phys.* **2017**, *19*, 32166–32178. DOI: 10.1039/C7CP06793C.

[12] Moradkhani, M.; Naghipour, A.; Abbasi Tyula, Y. A Theoretical Investigation of the Competition between σ- and π-Holes on the Stability of the Complexes Resulting from the Interaction between the COCl2 and OCY Molecules (Y = S, Se, and Te). *Phosp. Sulfur Silicon Relat. Elem.* **2024**, *199*, 486–495. DOI: 10.1080/10426507.2024.2378049.

[13] Isamura, B. K.; Lobb, K. A. New Insights into the (A)Synchronicity of Diels–Alder Reactions: A Theoretical Study Based on the Reaction Force Analysis and Atomic Resolution of Energy Derivatives. *Molecules* **2022**, *27*, 1546. DOI: 10.3390/molecules27051546.

[14] Lobb, K. A. Isomerization of the 2-Norbornyl Carbocation. *Eur. J. Org. Chem.* **2015**, *2015*, 5370–5380. DOI: 10.1002/ejoc.201500518.

[15] Alvarez-Idaboy, J. R.; Mora-Diez, N.; Vivier-Bunge, A. A Quantum Chemical and Classical Transition State Theory Explanation of Negative Activation Energies in OH Addition

To Substituted Ethenes. *J. Am. Chem. Soc.* **2000**, *122*, 3715–3720. DOI: 10.1021/ja993693w.
[16] Santoro, S.; Himo, F. Mechanism of the Kinugasa Reaction Revisited. *J. Org. Chem.* **2021**, *86*, 10665–10671. DOI: 10.1021/acs.joc.1c01351.
[17] Liu, D. Structural Tuning and Spectroscopic Characterizations of Polysulfide as Battery Materials. PhD Thesis, University of Western Ontario, **2021**. p. 49.
[18] Bulat, F. A.; Toro-Labbé, A.; Brinck, T.; Murray, J. S.; Politzer, P. Quantitative Analysis of Molecular Surfaces: Areas, Volumes, Electrostatic Potentials and Average Local Ionization Energies. *J. Mol. Model.* **2010**, *16*, 1679–1691. DOI: 10.1007/s00894-010-0692-x.
[19] Bondi, A. Van Der Waals Volumes and Radii. *J. Phys. Chem.* **1964**, *68*, 441–451. DOI: 10.1021/j100785a001.
[20] Li, R.; Zheng, J.; Truhlar, D. G. Density Functional Approximations for Charge Transfer Excitations with Intermediate Spatial Overlap. *Phys. Chem. Chem. Phys.* **2010**, *12*, 12697–12701. DOI: 10.1039/C0CP00549E.
[21] Csonka, G. I. Proper Basis Set for Quantum Mechanical Studies of Potential Energy Surfaces of Carbohydrates. *J. Mol. Struct. Theochem.* **2002**, *584*, 1–4. DOI: 10.1016/S0166-1280(02)00096-9.
[22] Geerlings, P.; De Proft, F. Conceptual DFT: The Chemical Relevance of Higher Response Functions. *Phys. Chem. Chem. Phys.* **2008**, *10*, 3028–3042. DOI: 10.1039/B717671F.
[23] van Duijneveldt, F. B.; van Duijneveldt-van de Rijdt, J. G. C. M.; van Lenthe, J. H. State of the Art in Counterpoise Theory. *Chem. Rev.* **1994**, *94*, 1873–1885. DOI: 10.1021/cr00031a007.
[24] Grev, R. S.; Janssen, C. L.; Schaefer, H. F., III, Concerning Zero-Point Vibrational Energy Corrections to Electronic Energies. *J. Chem. Phys.* **1991**, *95*, 5128–5132. DOI: 10.1063/1.461680.
[25] Glendening, E. D.; Landis, C. R.; Weinhold, F. Natural Bond Orbital Methods. *WIREs Comput. Mol. Sci.* **2012**, *2*, 1–42. DOI: 10.1002/wcms.51.
[26] Szalewicz, K. Symmetry-Adapted Perturbation Theory of Intermolecular Forces. *WIREs Comput. Mol. Sci.* **2012**, *2*, 254–272. DOI: 10.1002/wcms.86.
[27] https://ccdbdb.nist.gov/vsfx.asp.
[28] Frisch, M. J.; Trucks, G. W.; Schlegel, H. B.; Scuseria, G. E.; Robb, M. A.; Cheeseman, J. R.; Scalmani, G.; Barone, V.; Petersson, G. A.; Nakatsuji, H.; et al. *Fox, D. J. Gaussian 16, Revision C.01*, Wallingford CT: Gaussian, Inc., **2016**.
[29] Dennington, R.; Keith, T. A.; Millam, J. M.. *GaussView, Version 6.0. Shawnee Mission, KS*, USA: Semichem Inc., **2016**.
[30] Chemcraft – Graphical Software for Visualization of Quantum Chemistry Computations. *Version 1*. 2025, *8*, 682. https://www.chemcraftprog.com
[31] Bruker NMR Hardware User Guide (Emory.edu). 2021.